

## **A Numerical Investigation of the Thermal Performances of an Array of Heat Pipes for Battery Thermal Management**

**Chaoyi Wan<sup>1,\*</sup>**

**Abstract:** A comparative numerical study has been conducted on the thermal performance of a heat pipe cooling system considering several influential factors such as the coolant flow rate, the coolant inlet temperature, and the input power. A comparison between numerical data and results available in the literature has demonstrated that our numerical procedure could successfully predict the heat transfer performance of the considered heat pipe cooling system for a battery. Specific indicators such as temperature, heat flux, and pressure loss were extracted to describe the characteristics of such a system. On the basis of the distributions of the temperature ratio of the battery surface, together with the heat flux and the streamlines around the heat pipe condenser, we conclude that the low disturbance of the coolant is the cause of the temperature gradient along the fluid flow direction.

**Keywords:** Battery thermal management, heat pipe, numerical model, temperature difference.

### **1 Introduction**

The lithium-ion battery is promising energy storage equipment for electric vehicles and hybrid electric vehicles due to its high energy density [Choi and Kang (2014); Etacheri, Marom, Elazari et al. (2011)]. The optimum working temperature of the lithium battery is 25-40°C [Tran, Harmand and Sahut (2014); Rao, Wang, Wu et al. (2013); Waldmann, Wilka, Kasper et al. (2014); Bandhauer, Garimella and Fuller (2011)]. The maximum temperature difference should not exceed 5°C in one battery pack [Troxler, Wu, Marinescu et al. (2014); Wang, Tseng, Zhao et al. (2014)]. otherwise, it may cause serious safety problems [Troxler, Wu, Marinescu et al. (2014); Bandhauer, Garimella and Fuller (2011)]. The heat pipe cooling system, which uses liquid-gas phase change without consuming extra power, has become the most promising cooling method in lithium-ion battery thermal management systems, with excellent heat transfer performance and rapid response capability [Tran, Harmand and Sahut (2014); Rao, Wang, Wu et al. (2013); Greco, Cao, Jiang et al. (2014); Rao, Huo and Liu (2014)].

The power battery generates heat in excess of 50 W [Ye, Saw, Shi et al. (2015); Ye, Saw, Shi et al. (2014)], and more during acceleration and other high charging or discharging conditions. Rao et al. conducted experimental research which showed that the maximum

---

<sup>1</sup> School of Automobile and Traffic Engineering, Jiangsu University of Technology, Changzhou, 213001, China.

\* Corresponding Author: Chaoyi Wan. Email: wcyjust@163.com.

temperature of the battery surface can be controlled below 50°C when heat generation of the battery is less than 50 W [Rao, Wang, Wu et al. (2013)]. However, the maximum temperature difference is approximately 8°C. The heat load should not exceed 30 W to maintain the surface temperature difference within 5°C. The experimental study of Wang et al. pointed out that the battery temperature can stay below 70°C when the heat generation per cell is between 20-40 W or, the amount of heat generation cannot exceed 10 W in order to retain the maximum temperature below 40°C [Wang, Jiang, Xue et al. (2015)]. Ye et al. found that the heat transfer coefficient of the heat pipe condenser surface decreased significantly along the flow passage, causing unevenness of the battery temperature. Dummy heat pipes and copper fins could enhance the heat transfer and temperature uniformity [Ye, Saw, Shi et al. (2015)]. Ye et al. also pointed out that the addition of fins at the heat pipe condenser sections have a significant effect on lowering the maximum temperature and the temperature difference on the battery surface [Ye, Shi, Saw et al. (2016)].

These studies lacked severe working conditions such as the heat pipe cooling system integrated with batteries charged at high input power. A detailed temperature distribution of the battery surface is also required to explain the mechanism that causes the temperature difference. In this study, numerical investigations were conducted on heat transfer characteristics and flow details in a heat pipe cooling system for lithium batteries. The validity of the numerical models and grids used in this study was carefully checked and calibrated by comparing them with experimental data in the literature. Amounts of indicators such as temperature, heat flux, and pressure loss were extracted to characterize the heat performance of the heat pipe cooling system with batteries charged at high input power. The temperature distributions of the battery surface were also displayed to explain the effect of the coolant flow rate, coolant inlet temperature, and input power on the temperature uniformity of the battery surface.

## **2 Numerical setups**

### ***2.1 Geometry models and simplifications***

Fig. 1 shows a configuration of the heat pipe cooling system for a prismatic battery pack. Between two prismatic batteries (118 mm×63 mm×13 mm) sandwiched evaporator sections of four heat pipes. The heat generated in the battery was transferred to the condenser section through the heat pipe and then emitted into the coolant flow through the cooling passage (300 mm×60 mm×12 mm). Each heat pipe was flattened from a tubular condenser ( $\Phi=6.0\text{mm}$ ) to a rectangular evaporator Section (2.0mm×8.5mm). The geometrical parameters of batteries and the cooling channel are listed in Tab. 1.

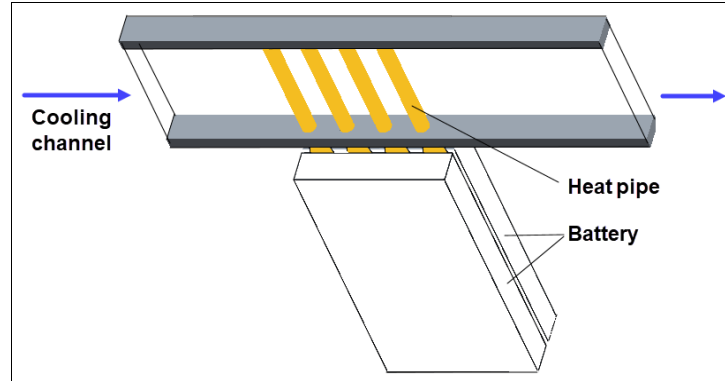


**Figure 1:** Configuration of the heat pipe cooling system for a prismatic battery pack

**Table 1:** Parameters of the heat pipe cooling system for the battery

Parameters of the heat pipe cooling system for the prismatic battery		
$l_t$	The total length of the heat pipe (m)	0.198
$l_c$	Length of condenser section (m)	0.06
$l_{ad}$	Length of adiabatic section (m)	0.02
$l_e$	Length of evaporator section (m)	0.118
$r_c$	Cross section radius of the copper shell (m)	0.003
$r_i$	Inner chamber radius (m)	0.0026
$r_v$	Cross section radius of vapor core (m)	0.002
$\varepsilon$	Porosity ( )	0.50

It is complex and time-consuming to model all details for a battery pack cooled by heat pipe for phase changes and other phenomena in heat pipes. Even in the case of simulating one heat pipe, high computational resources are necessary to characterize the mass and heat transfer during transient charging or discharging of the cell. Thus, a more efficient approach for numerical computation was adopted. The thermal behavior of a heat pipe on battery cooling would be treated as a thermal network of various components, and then the transient behavior could be described by first order linear ordinary differential equations [Zuo and Faghri (1998)]. Solving electro-chemical reactions of a battery was also too complicated for only presenting the thermal behavior of battery cell (multi-layer structure). Therefore, a simplified model without considering electro-chemical reactions was applied to present the heat generation of the battery, as well as the thermal properties of a multi-layered battery cell. This approach was well validated by comparisons with experimental and numerical studies and has been applied in numerous studies [Choi and Kang (2014); Greco, Cao, Jiang et al. (2014); Ye, Saw, Shi et al. (2015); Zuo and Faghri (1998)].

## 2.2 Model formulation of the heat pipe

### 2.2.1 Copper shell

The thermal properties of copper were applied directly to the copper shell during this simulation because the heat transfer through the copper shell of the heat pipe was entirely conduction.

### 2.2.2 Wick region

In this study, a heat pipe with a higher maximum heat transfer limit than the target heat load has been selected to avoid drying during operation. The heat pipes employed in the study had the minimum total heat transfer limit of 200 W, which was the capillary limit. The wick region was considered to be a porous structure filled with water. A widely accepted model developed by Chi [Chi (1976)] can be used to calculate the effective thermal conductivity of the wick region  $k_{wick}$ :

$$k_{wick} = \frac{k_l[(k_l + k_s) - (1 - \varepsilon)(k_l - k_s)]}{[(k_l + k_s) + (1 - \varepsilon)(k_l - k_s)]} \quad (1)$$

where  $k_l$  and  $k_s$  are the thermal conductivity of working fluid and sintered copper powder porous wick, respectively, and  $\varepsilon$  is the porosity. In this study, the effective thermal conductivity of the wick region was calculated to be  $1.814 \text{ Wm}^{-1}\text{K}^{-1}$ .

The volumetric averaged density of the mixture of water and sintered copper powder porous wick could be utilized to determine to the density of the wick region by Eq. (2), and the specific heat capacity was obtained according to Eq. (3).

$$\rho_{wick} = \varepsilon\rho_l + (1 - \varepsilon)\rho_s \quad (2)$$

$$C_{wick} = [\varepsilon\rho_l C_l + (1 - \varepsilon)\rho_s C_s] / \rho_{wick} \quad (3)$$

where  $\rho_{wick}$ ,  $\rho_l$ ,  $\rho_s$  are the densities of the wick, working fluid and copper powder, respectively,  $C_{wick}$ ,  $C_l$ ,  $C_s$  are the specific heat capacity of the wick, working fluid and copper powder, respectively, and  $\varepsilon$  is the porosity.

### 2.2.3 Vapor core

The vapor flow was considered incompressible, laminar and fully developed. By assuming the relationship between pressure drop and temperature drop in accordance with the Clapeyron equation and the ideal gas law [Prasher (2003); Wei and Sikka (2006)], the effective thermal conductivity of the vapor core in a tubular heat pipe can be calculated by Eq. (4) [Prasher (2003)].

$$k_{vapor} = \frac{r_v^2 L^2 \rho_v P_v}{8\mu RT^2} \quad (4)$$

where  $r_v$  is the cross-section radius of the vapor core.  $L$  is the latent heat of working fluid.  $\rho$ ,  $P_v$ ,  $\mu$ ,  $R$  and  $T$  is the density, the saturation pressure, the dynamic viscosity,

the gas constant per unit mass and the temperature of the water vapor, respectively. The  $k_{\text{vapor}}$  was calculated as  $4.69 \times 10^6 \text{ W m}^{-1} \text{ K}^{-1}$  using the properties of saturated water vapor at a temperature of  $40^\circ\text{C}$ .

### **2.3 Thermal model of the battery**

Two aluminum blocks of the same size as some commercial power batteries were used to simulate batteries [Rao, Wang, Wu et al. (2013); Wang, Jiang, Xue et al. (2015); Ling, Chen, Fang et al. (2014); Liang, Gan and Li (2018)]. It was assumed that during the entire operation process, the heat generation rate of the battery was a constant value which was regarded as the maximum power during the highest sustainable constant-current discharge rate. In this study, the heat generation rate was in the range of 20-80 W per cell.

### **2.4 Numerical procedures**

In this calculation, numerical studies were performed by the commercial CFD software-ANSYS Workbench 17.2 FLUENT using a local parallel solver in a double precision mode. Heat radiation transfer is negligible and was not considered.

Block-structured grids with hexahedral elements were employed to realize the spatial discretization of the domain models. Cell orthogonality was ensured by introducing multiple O-grid blocks for heat pipes. Denser grids were applied in the non-slip boundary regions where the flow and temperature gradients are higher meaning, the area around heat pipes and the end wall of the coolant channel. The grid independence test was performed by gradually refining the mesh size to ensure that the mesh size has little impact on the results. When cell number changed from 2628477 cells to 4737970 cells then to 7895174, the maximum temperature changed from  $43.57^\circ\text{C}$  to  $42.59^\circ\text{C}$  then  $42.49^\circ\text{C}$ , respectively. While continuing to increase the number of grids, the maximum temperature was kept almost constant. According to the procedure described [Celik, Ghia, Roache et al. (2008)], the grid convergence index (GCI) of the maximum temperature was 2.81%. Fig. 2 shows the mesh used in this numerical investigation.

All materials, boundary conditions, and data processing methods were modified according to the experiment of Liang et al. [Liang, Gan and Li (2018)]. The computation models included the heat transfer in the solid wall and in the fluid, which was coupled to solve energy equations automatically. The surface of the channel and the insulation section of heat pipes were treated as isolation and no-slip boundaries. The two batteries had a constant volume heat generation rate. At the inlet of the channel, constant velocity was applied. Laminar was used to calculate the viscous due to the inlet Reynolds number.

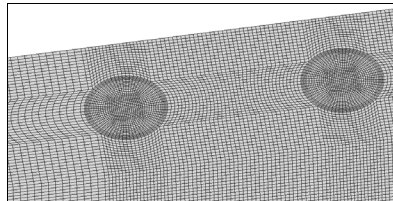


**Figure 2:** Hexahedral mesh used in the present numerical study

### 3 Model validation

The results obtained by the computation procedure compared favorably with the published experimental data of Liang et al. [Liang, Gan and Li (2018)]. Data are plotted in Fig. 3 for comparison. In Fig. 3,  $T_c$  is the coolant inlet temperature,  $T_{ab}$  is the ambient temperature, and  $T_{max}$  is the maximum temperature of the battery surface. As illustrated, the maximum deviation between the numerical computation results in this research and the data from the literature [Liang, Gan and Li (2018)] were kept within 10%. Based on the above validation, the numerical model was considered to be reliable and can be applied to predict the heat performance of the heat pipe cooling system for the battery.

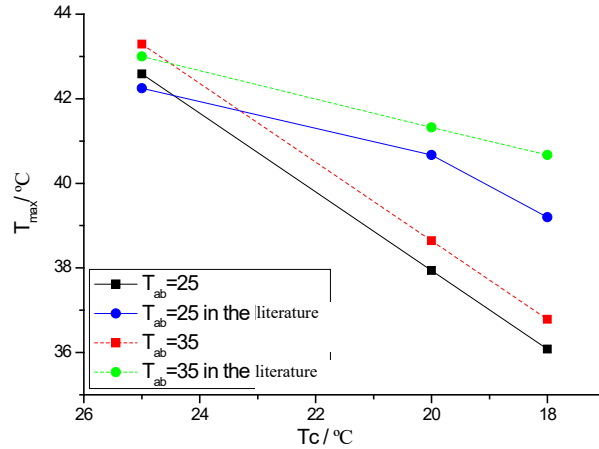


**Figure 3:** Results of maximum temperature varied with coolant inlet temperature obtained by CFD and experimental data from Liang et al. [Liang, Gan and Li (2018)] for comparison

## 4 Results and discussion

### 4.1 Effects of coolant flow rate

In this section, the effect of the coolant flow rate of the heat pipe cooling system on the temperature of the battery surface is discussed. The input power was set at 40 W/cell while the coolant inlet temperature  $T_c$  was set as 25°C. The cooling flow rate for the study ranged from 0.5 L/min to 8 L/min. The maximum temperature ( $T_{max}$ ), average temperature ( $T_{avg}$ ), and temperature difference ( $\Delta T$ ) of battery surface with different coolant flow rates are shown in Fig. 4.

Both  $T_{max}$  and  $T_{avg}$  reduced with the increased coolant flow rate. Notably, when the coolant flow rate reaches some specific value, the trend of reduction tends to be very gentle. This is consistent with the results presented in other studies [Ye, Saw, Shi et al. (2015); Liang, Gan and Li (2018); Zhao, Lv and Rao (2017)]. While the coolant flow rate changes from 0.5 L/min to 2 L/min, the maximum temperature decreases approximately 8.9°C, which is approximately 16.9%. While the coolant flow rate changes from 2 L/min to 8 L/min, the maximum temperature decreases approximately 4.07°C, which is approximately 9.3%. As

the coolant flow rate increases, the pressure loss ( $\Delta P$ ) increases dramatically from 1.35 Pa to 77.76 Pa. When considering that the pressure loss increases significantly with the coolant flow rate (Fig. 5), this indicates that it is not feasible to enhance the thermal performance of the heat pipe cooling system by merely increasing the coolant flow rate. Therefore, other approaches should be considered to reduce the battery temperature.

The temperature difference of the battery surface  $\Delta T$  decreases as the coolant flow rate increases (Fig. 4). The distribution of temperature ratio ( $T/T_{avg}$ ) can represent the temperature difference, and that of the battery surface with different coolant flow rates (Fig. 6). The temperature gradient along the length of heat pipes is caused by heat conduction from bottom to top, and the temperature gradient along the coolant streamwise is very likely resulting from a reduction in the effective heat transfer coefficient in the flow direction. The increasing coolant flow rate enhances the disturbance of the coolant, which enhances the mixing of hot water around the heat pipe condensers and the cold water on the periphery. It contributes to the increase of the effective heat transfer coefficient in the flow direction and the reduction of the temperature gradient downstream of the coolant.

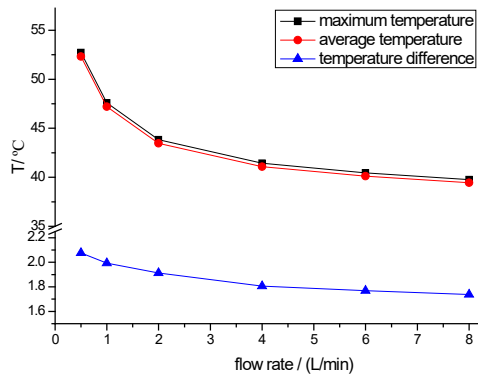


**Figure 4:**  $T_{max}$ ,  $T_{avg}$ , and  $\Delta T$  of battery with different coolant flow rates (input power is 40 W/cell under  $T_c = 25^\circ C$ )

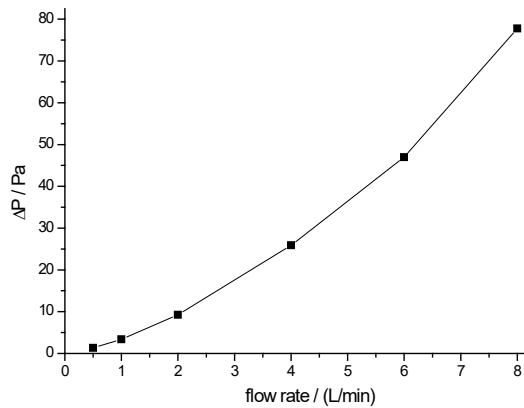


**Figure 5:** Pressure loss of the cooling channel with different coolant flow rates

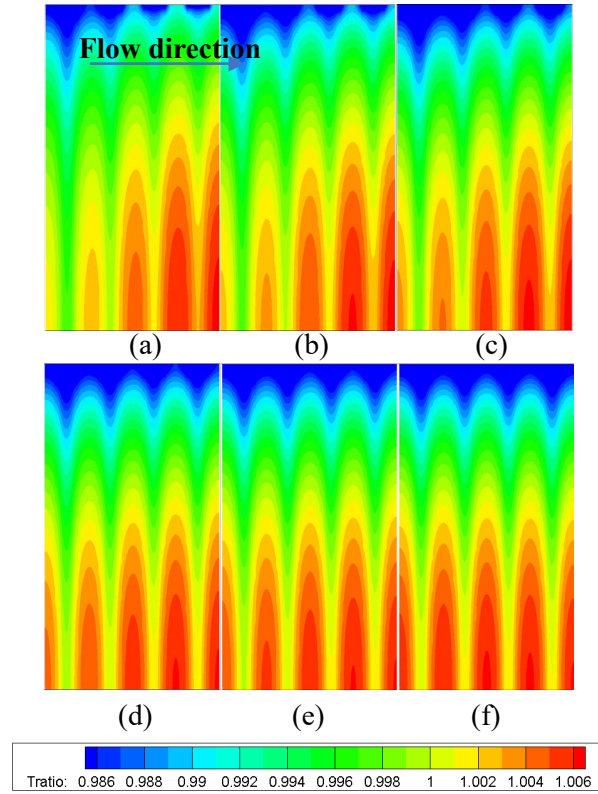


**Figure 6:** Distribution of temperature ratio ( $T/T_{avg}$ ) of battery with different coolant flow rates (a)  $q_v = 0.5L/min$ , (b)  $q_v = 1L/min$ , (c)  $q_v = 2L/min$ , (d)  $q_v = 4L/min$  (e)  $q_v = 6L/min$ , and (f)  $q_v = 8L/min$

#### 4.2 Effect of coolant inlet temperature

As discussed in the previous section, the effect of coolant flow rate is not apparent when the coolant flow rate reaches a specific value while further increasing the flow rate and resulting in a significant increase in pressure loss. Reducing the coolant inlet temperature is an effective method. For studying the effect of coolant inlet temperature on the heat pipe cooling system, the input power was set at 40 W/cell, while the coolant flow rate was set at 2 L/min. The coolant inlet temperature ranged from 25°C to 45°C. The maximum temperature ( $T_{max}$ ), average temperature ( $T_{avg}$ ), and temperature difference ( $\Delta T$ ) of battery surface under different coolant inlet temperatures is shown in Fig. 7.

Both  $T_{max}$  and  $T_{avg}$  increase linearly as the coolant inlet temperature increases. The maximum temperature  $T_{max}$  increases from 33.91°C to 53.91°C as the coolant inlet temperature increases from 15°C to 35°C. The temperature uniformity is less affected by coolant inlet temperature. The temperature difference ( $\Delta T$ ) is always approximately 1.9°C.

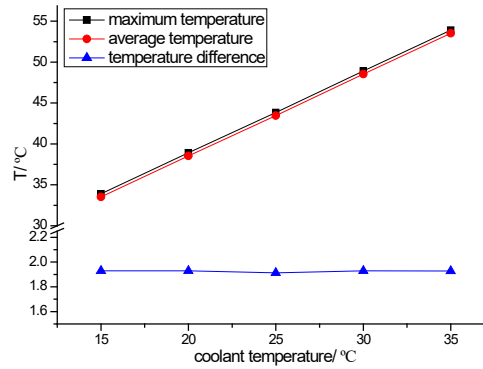


**Figure 7:**  $T_{\max}$ ,  $T_{\text{avg}}$  and  $\Delta T$  of battery with different coolant inlet temperatures (input power is 40 W/cell under  $q_v = 2L / \text{min}$ )

### 4.3 Effect of input power

In this section, the effect of input power on the temperature of the battery surface is investigated. The cooling flow rate was set at 2 L/min under  $T_c = 25^\circ\text{C}$ , and the input power ranged from 20 W to 80 W. The maximum temperature ( $T_{\max}$ ), average temperature ( $T_{\text{avg}}$ ), and temperature difference ( $\Delta T$ ) of battery surface with different input powers of the battery are shown in Fig. 8.

$T_{\max}$ , and  $T_{\text{avg}}$  as well as  $\Delta T$  significantly increase as the input power increases (Fig. 8). While the input power changes from 20 W to 80 W, the maximum temperature increases from 34.38°C to 62.97°C, and the temperature difference increases from 0.96°C to 3.86°C. Fig. 9 illustrates that the increase in  $\Delta T$  is mainly due to an increase in the temperature gradient along the heat pipe which is caused by heat conduction from the bottom to the top.

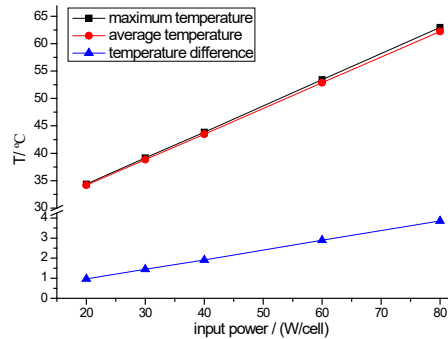


**Figure 8:**  $T_{\max}$ ,  $T_{\text{avg}}$ , and  $\Delta T$  of battery with different input power (mass flow rate  $q_v = 2L / \text{min}$  under coolant inlet temperature  $T_c = 25^\circ\text{C}$ )

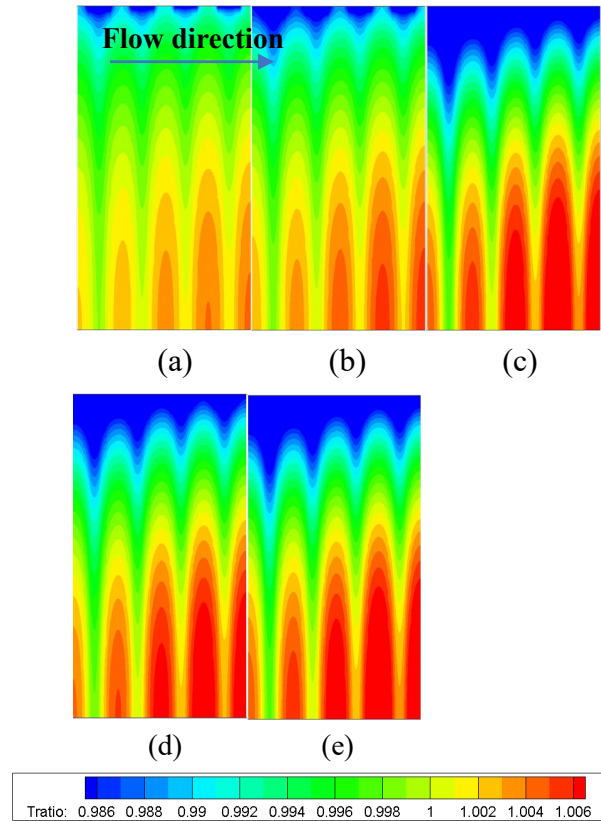


**Figure 9:** Distribution of temperature ratio ( $T/T_{avg}$ ) of the battery with different input power (a)  $P = 20W / cell$  (b)  $P = 30W / cell$  (c)  $P = 40W / cell$  (d)  $P = 60W / cell$  (e)  $P = 80W / cell$

As previously discussed, the optimum working temperature of the lithium battery is between 25°C and 40°C [Tran, Harmand and Sahut (2014); Rao, Wang, Wu et al. (2013); Waldmann, Wilka, Kasper et al. (2014); Bandhauer, Garimella and Fuller (2011)], and the maximum temperature difference in the same battery pack should not exceed 5°C [Troxler, Wu, Marinescu et al. (2014); Wang, Tseng, Zhao et al. (2014)]. Thus, for this configuration of the heat pipe cooling system of  $q_v = 2L / min$  and  $T_c = 25^\circ C$ , the maximum input power should not exceed 30 W for controlling the maximum temperature of the cooling surface below 40°C.

#### 4.4 Correlation to predict the maximum temperature

For the scope of this study, the maximum temperature  $T_{max}$  can be predicted using a correlation consisting of coolant inlet temperatures, coolant flow rate and input power, and is provided below:

$$T_{\max} = 48.121 * q_v^{(-0.1)} + T_c + 0.5 * P - 45.4 \quad (5)$$

where  $T_{\max}$  is the maximum temperature of the battery surface, °C;  $q_v$  is the coolant flow rate, L/min;  $T_c$  is the coolant inlet temperatures, °C; and  $P$  is the input power of each cell, W.

The results are listed in Tab. 2. For the scope of this study, the maximum deviation between the correlation results and the CFD results is -2.96%. Outside the scope of this study, the accuracy of the correlation requires further verification.

**Table 2:** Results of the maximum temperature  $T_{\max}$  obtained by the CFD and the correlation

$q_v$	$T_c$	$P$	CFD (°C)	Correlation (°C)	Deviation (%)
0.5	25	40	52.7	51.2	-2.96
1	25	40	47.6	47.7	0.26
2	25	40	43.8	44.5	1.5
4	25	40	41.4	41.5	0.15
6	25	40	40.4	39.8	-1.52
8	25	40	39.8	38.7	-2.73
2	15	40	33.9	34.5	1.74
2	20	40	38.9	39	1.51
2	30	40	48.9	49.5	1.2
2	35	40	53.9	54.5	1.1
2	25	20	34.4	34.4	0.06
2	25	30	39.1	39.5	0.91
2	25	60	53.4	54.5	1.99
2	25	80	63	64.5	2.43

#### 4.5 Heat transfer distribution in the heat pipe condenser sections

Due to the high conductivity of heat pipes, the thermal performance of the heat pipe cooling system is significantly affected by the convective heat transfer between the coolant and the heat pipe condenser section. As shown in Figs. 6 and 9, the maximum temperature occurs in the region downstream of the flow direction away from the cooling channel, and the minimum temperature is in the opposite diagonal region that is, the upstream flow direction near the cooling channel. A temperature gradient occurs both along the heat pipe and the fluid flow direction. The temperature gradient along the length of the heat pipes is caused by heat conduction from bottom to top, and the temperature gradient along the coolant streamwise very likely results from a reduction in the effective heat transfer coefficient in the flow direction.

Fig. 10 displays the convective heat transfer coefficient at the wall of the heat pipe

condenser section in the flow direction and streamlines in the cooling channel while the coolant flow rate was  $q_v = 2\text{ L/min}$  under coolant inlet temperature  $T_c = 25\text{ }^\circ\text{C}$ , and the input power of the battery was  $40\text{ W/cell}$ . It can be seen that the cold coolant first crashed on the primary heat pipe then exchanged great heat. The region of the battery surface connected to the primary heat pipe became colder and the coolant became warmer. The flow was mainly laminar, and fewer vortices were produced in the flow field, which inhibited the mixing of warmer water around the heat pipe and colder water in the periphery. Lower temperature differences between the coolant and the heat pipe condenser section reduced the convective heat transfer coefficient downstream from the second to the fourth heat pipe. A comprehensive investigation of how to increase the disturbance in the coolant channel to decrease the temperature gradient along the coolant streamwise will be our next research focus.

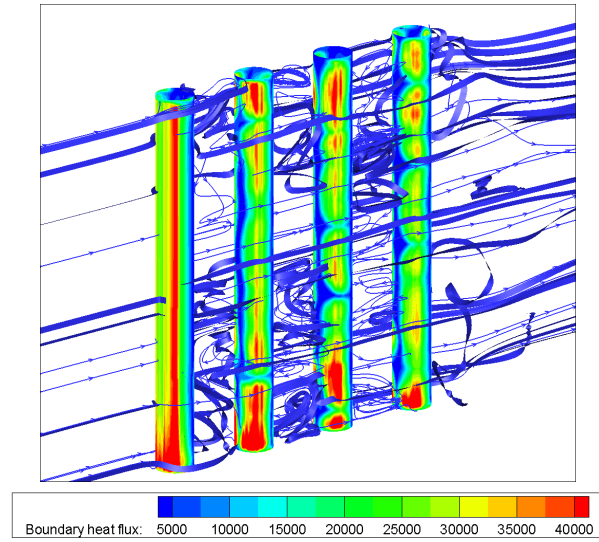


**Figure 10:** Streamline and Nusselt number on the heat pipe condenser section

## 5 Conclusion

In the present study, the thermal performance of the heat pipe cooling system was discussed by taking the effects of coolant flow rate, coolant inlet temperature and input power using numerical methods. Numerical models and procedures were carefully validated and calibrated with experimental results from the literature. The model and approach demonstrated considerable accuracy and was then subjected to a sensitivity analysis. Amounts of indicators such as temperature, heat flux, and pressure loss were extracted to describe the characteristics of the heat pipe cooling system. The results of this study can provide some useful guidance for the heat pipe cooling system. Several main conclusions can be drawn and are as follows:

(1) Referring to the configuration of the heat pipe cooling system, the temperature of the battery decreased with the increase of the coolant flow rate until it reached  $2\text{ L/min}$ , and then the reduction was not significant. It also increased significantly as the coolant inlet

temperature and the input power increased.

(2) Regarding the configuration of the heat pipe cooling system, the temperature difference decreased as the coolant flow rate increased, and increased significantly as the input power increased, while the temperature uniformity was less affected by the coolant inlet temperature.

(3) A correlation consisting of coolant inlet temperatures, coolant flow rate and input power was provided to predict the maximum temperature  $T_{\max}$  for the configuration of the heat pipe cooling system in the scope of this study. The maximum deviation between the CFD results and the correlation results were -2.96%.

(4) The convective heat transfer coefficient at the wall of the heat pipe condenser section and the streamlines in the cooling channel indicated that the low disturbance of the coolant is the cause of the temperature gradient along the fluid flow direction.

**Acknowledgments:** This work was supported by the Natural Science Foundation of Jiangsu Province (Grants No. BK20170317).

## Reference

**Bandhauer, T. M.; Garimella, S.; Fuller, T. F.** (2011): A critical review of thermal issues in lithium-ion batteries. *Journal of the Electrochemical Society*, vol. 158, no. 3, pp. R1-R25.

**Celik, I.; Ghia, U.; Roache, P.; Freitas, C.; Coleman, H. et al.** (2008): Procedure for estimation and reporting of uncertainty due to discretization in CFD applications. *Journal of Fluids Engineering*, vol. 130, no. 7, pp. 078001.

**Chi, S.** (1976): *Heat Pipe Theory and Practice: A Sourcebook*.

**Choi, Y. S.; Kang, D. M.** (2014): Prediction of thermal behaviors of an air-cooled lithium-ion battery system for hybrid electric vehicles. *Journal of Power Sources*, vol. 270, no. 2014, pp. 273-280.

**Etacheri, V.; Marom, R.; Elazari, R.; Salitra, G.; Aurbach, D.** (2011): Challenges in the development of advanced Li-ion batteries: a review. *Energy & Environmental Science*, vol. 4, no. 9, pp. 3243-3262.

**Greco, A.; Cao, D.; Jiang, X.; Yang, H.** (2014): A theoretical and computational study of lithium-ion battery thermal management for electric vehicles using heat pipes. *Journal of Power Sources*, vol. 257, no. 2014, pp. 344-355.

**Liang, J.; Gan, Y.; Li, Y.** (2018): Investigation on the thermal performance of a battery thermal management system using heat pipe under different ambient temperatures. *Energy Conversion and Management*, vol. 155, no. 2018, pp. 1-9.

**Ling, Z.; Chen, J.; Fang, X.; Zhang, Z.; Xu, T. et al.** (2014): Experimental and numerical investigation of the application of phase change materials in a simulative power batteries thermal management system. *Applied Energy*, vol. 121, no. 2014, pp. 104-113.

**Prasher, R. S.** (2003): A simplified conduction based modeling scheme for design

sensitivity study of thermal solution utilizing heat pipe and vapor chamber technology. *Journal of Electronic Packaging*, vol. 125, no. 3, pp. 378-385.

**Rao, Z.; Huo, Y.; Liu, X.** (2014): Experimental study of an OHP-cooled thermal management system for electric vehicle power battery. *Experimental Thermal and Fluid Science*, vol. 57, no. 2014, pp. 20-26.

**Rao, Z.; Wang, S.; Wu, M.; Lin, Z.; Li, F.** (2013): Experimental investigation on thermal management of electric vehicle battery with heat pipe. *Energy Conversion and Management*, vol. 65, no. 2013, pp. 92-97.

**Tran, T. H.; Harmand, S.; Sahut, B.** (2014): Experimental investigation on heat pipe cooling for Hybrid Electric Vehicle and Electric Vehicle lithium-ion battery. *Journal of Power Sources*, vol. 265, no. 2014, pp. 262-272.

**Troxler, Y.; Wu, B.; Marinescu, M.; Yufit, V.; Patel, Y. et al.** (2014): The effect of thermal gradients on the performance of lithium-ion batteries. *Journal of Power Sources*, vol. 247, no. 2014, pp. 1018-1025.

**Waldmann, T.; Wilka, M.; Kasper, M.; Fleischhammer, M.; Wohlfahrt-Mehrens, M.** (2014): Temperature dependent ageing mechanisms in Lithium-ion batteries-a post-mortem study. *Journal of Power Sources*, vol. 262, no. 2014, pp. 129-135.

**Wang, Q.; Jiang, B.; Xue, Q. F.; Sun, H. L.; Li, B. et al.** (2014): Experimental investigation on EV battery cooling and heating by heat pipes. *Applied Thermal Engineering*, vol. 88, no. 2015, pp. 54-60.

**Wang, T.; Tseng, K. J.; Zhao, J.; Wei, Z.** (2014): Thermal investigation of lithium-ion battery module with different cell arrangement structures and forced air-cooling strategies. *Applied Energy*, vol. 134, no. 2014, pp. 229-238.

**Wei, X.; Sikka, K.** (2006). Modeling of vapor chamber as heat spreading devices. *Conference on Thermal & Thermomechanical Phenomena in Electronics Systems. IEEE*.

**Ye, Y.; Saw, L. H.; Shi, Y.; Somasundaram, K.; Tay, A. A.** (2014): Effect of thermal contact resistances on fast charging of large format lithium ion batteries. *Electrochimica Acta*, vol. 134, no. 2014, pp. 327-337.

**Ye, Y.; Saw, L. H.; Shi, Y.; Tay, A. A.** (2015): Numerical analyses on optimizing a heat pipe thermal management system for lithium-ion batteries during fast charging. *Applied Thermal Engineering*, vol. 86, no. 2015, pp. 281-291.

**Ye, Y.; Shi, Y.; Saw, L. H.; Tay, A. A.** (2016): Performance assessment and optimization of a heat pipe thermal management system for fast charging lithium ion battery packs. *International Journal of Heat and Mass Transfer*, vol. 92, no. 2016, pp. 893-903.

**Zhao, J.; Lv, P.; Rao, Z.** (2017): Experimental study on the thermal management performance of phase change material coupled with heat pipe for cylindrical power battery pack. *Experimental Thermal and Fluid Science*, vol. 82, no. 2017, pp. 182-188.

**Zuo, Z.; Faghri, A.** (1998): A network thermodynamic analysis of the heat pipe. *International Journal of Heat and Mass Transfer*, vol. 41, no. 11, pp. 1473-1484.